Shape phase transition in $^{144-152}$Nd isotopes

J. B. Gupta
Ramjas College, University of Delhi, Delhi-110007, India
(Received 15 July 2015; published 19 October 2015)

Background: The $Z = 60$ $^{144-152}$Nd isotopes span the spherical to the well-deformed collective nuclear structures. The shape phase transition at $N = 86$–88 and $N = 88$–90 is intermediate between (Ba,Ce) and (Sm,Gd). The role of the $Z = 64$ subshell closure in this forms an interesting subject of study.
Objective: To analyze these complex features of the Nd spectra and the effects of the $Z = 64$ subshell by comparing with predictions from the microscopic dynamic pairing plus quadrupole model to explain the shape transition at $N = 86$–90.
Method: Empirical analysis of the Nd spectra is illustrated. The K-band structures of the collective $I^\pi = 2^+$ states in $^{144-152}$Nd are described. The predicted $B(E2)$ values and the interband $B(E2)$ ratios are compared with experimental data. The potential-energy surfaces of $^{146-152}$Nd are illustrated, and the role of protons and neutrons filling the Nilsson orbits is described.
Results: The different effects of the $Z = 64$ subshell on the ground-state band and the excited vibrational bands of $^{146-148}$Nd are illustrated.
Conclusion: The important role of the dynamics of the nucleus, besides the static features, is made more transparent.

DOI: 10.1103/PhysRevC.92.044316 PACS number(s): 21.60.Ev, 21.60.Fw, 21.10.Re, 27.60.+j

I. INTRODUCTION

The light ($A = 144$–152) lanthanides are among the heavy nuclei with neutron excesses of more than a few units from the β-stability line that can be produced today. These are produced in the low-energy fission of heavy neutron-rich actinides. With five valence proton pairs above the $Z = 50$ closed shell, the $Z = 60$ $^{144-152}$Nd isotopes span the spherical to the well-deformed collective nuclear structures. The energy ratio $R_{4/2}(=E_4/E_2)$, a good measure of the nuclear core deformation independent of the nuclear mass, varies from 1.89 to 3.26 for the $N = 84$–92 Nd isotopes in quadrant 1 of the $Z = 50$–82 major shell. A plot of the ratio $R_{4/2}$ for the $N = 86, 88$, and 90 isotones versus Z, across the Ba-Hf nuclei (Fig. 1), illustrates the relative importance of the $^{146-150}$Nd isotopes. The profound dependence of the shape transition at $N = 86$, 88, and 90 isotones on the proton number Z exhibited here offers an interesting area of study for the nuclear structure theory. The sharpness of the shape phase transition at $N = 88$–90 for the Nd isotopes lies in between the (Ba,Ce) isotopes and the (Sm,Gd) isotopes. This is also the case at $N = 86$–88 for (Ba,Ce,Nd) and (Sm,Gd) [1] (Fig. 1).

Over the past four decades, numerous studies of the $^{144-152}$Nd isotopes have been performed, and information on the energy levels and the transition rates has become available [2]. The lowest few collective energy levels, grouped into the $K^\pi = 0_1^+$ ground, $K^\pi = 0_2^+ \beta_-$, and $K^\pi = 2^+\gamma$ bands are usually studied in the evolving collective nuclear models. With the advent of the algebraic $L = 0, 2$ sd-interacting boson models (IBM-1 and IBM-2) [3], new insights in the interpretation of the data have been possible. The three dynamic symmetries [3] of U(5), SU(3), and O(6) enable the association of the specific Nd isotopes with these symmetries. The $^{144-152}$Nd isotopes lie on the U(5)-SU(3) path, corresponding to the axially symmetric deformed shape transition. The $Z = 64$ subshell effects have been invoked [4] to explain the anomalous dependence of the structure on the proton number Z at $N = 86, 88$. The $Z = 64$ subshell effects are visible in $N = 88$ ^{148}Nd since $R_{4/2}$ drops from 2.65 in ^{144}Ba to 2.50 in ^{148}Nd, which drops further in ^{150}Sm and ^{152}Gd.

The identification of the analytically solvable critical point symmetry X(5) at the edge of the spherical to the axially symmetric deformed ($A = 150$–200) region [5] (except for the scaling factors) led to the recognition of ^{150}Nd as a possible candidate for the X(5) symmetry [6]. Clark *et al.* [7] studied the validity of the X(5) symmetry for ^{150}Nd and other $N = 90$ isotones. IBM-2 was employed to study the variation in nuclear structure with N for the Nd isotopes in Refs. [8,9,10]. In these works, the shape transition with varying neutron number N is illustrated, and the effect of the $Z = 64$ subshell is taken into account by using the reduced proton boson numbers N_p. The relativistic energy density-functional framework, using a five-dimensional quadrupole vibrator, was applied by Li *et al.* [11] to study the variation in the intrinsic shape $V(\beta, \gamma)$ in Nd isotopes with N. The self-consistent Hartree-Fock-Bogoliubov (HFB) approximation based on the finite-range and density-dependent Gogny interaction (parametrization DIS) has been used to generate potential-energy curves (PECs) in Nd isotopes and other nuclides by Robledo *et al.* [12].

The nuclear structure of the near U(5) symmetry nucleus ^{144}Nd was studied earlier in the microscopic dynamic pairing plus quadrupole model (DPPQM) [13] by Gupta [14]. The IBM-1 was used to analyze the variation in the nuclear structure of $^{146-150}$Nd with neutron number N in Ref. [15]. Recently, the special characters of the $N = 86$ isotones of (Ce, Nd, Sm, and Gd) were reported in Ref. [16] using the IBM-1 and the DPPQ models [13]. Using the updated data [2] (including revised information for $^{148-152}$Nd from Nucl. Data Sheets up to the year 2014), in the present paper, I extend the application of the DPPQ model to the

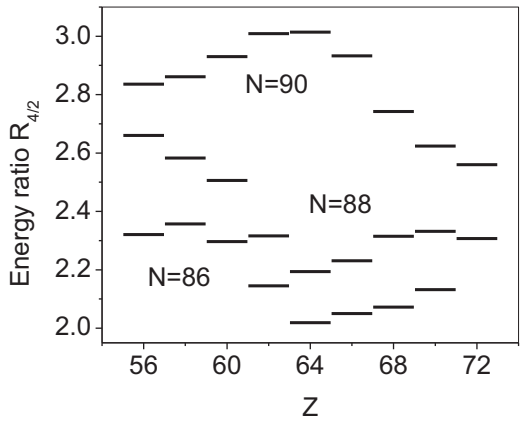

FIG. 1. Energy ratio $R_{4/2}$ versus Z for $N = 86, 88$, and 90 isotones of Ba-Hf.

heavier $^{148-152}$Nd isotopes. In Sec. II the ground-band data are analyzed empirically, and the special features of the $N = 86$–90 region are illustrated for Nd isotopes. A brief introduction to the IBM-1 and DPPQ model is given in Sec. III. In Sec. IV, the predictions from the IBM and the DPPQ model are compared with the experimental data. A summary and conclusion are given in Sec. V.

II. EMPIRICAL ANALYSIS OF THE LEVEL STRUCTURE OF $^{144-152}$Nd

A. Ground-state band

For Nd, the shape transition at $N = 88$–90 is much sharper than for $N = 86$–88 (Fig. 1). This is further highlighted in the plots of the energy ratio $R_{I/2}(= E_I/E_2)$ versus spin I in Fig. 2. This is in contrast to ^{144,146}Ba isotopes for which there is almost no shape transition at $N = 88$–90 as illustrated recently in Ref. [17].

Using the empirical two-term rotation-vibration formula,

$$E_I = aI + bI(I+1), \tag{1}$$

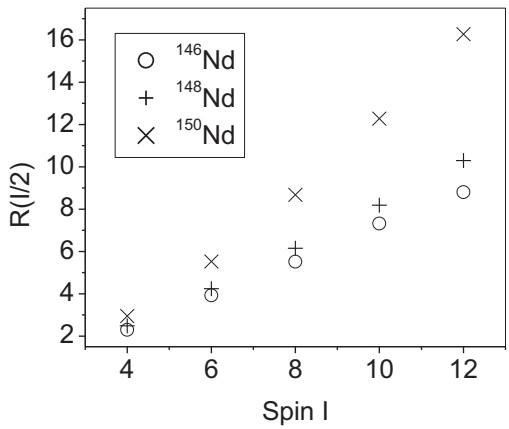

FIG. 2. Energy ratio $R_{I/2}(= E_I/E_2)$ in the ground bands of $^{146-150}$Nd.

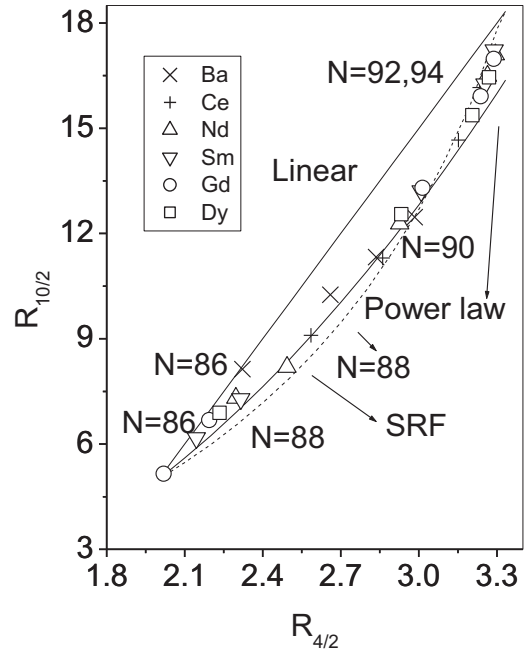

FIG. 3. The plot of $R_{10/2}$ versus $R_{4/2}$. The straight line is due to Eq. (2). The SRF values are on the dashed curve, and the power-law values are on the continuous curve. The symbols are experimental data.

one can derive the linearity relation of $R_{I/2}$ with $R_{4/2}$,

$$R_{I/2} = R_{4/2}[I(I-2)/8] - [I(I-4)/4]. \tag{2}$$

Up to spin $I^\pi = 10^+$, generally for a medium mass nuclide, one gets a regular energy-level sequence. Hence it can serve as a good measure for the structure of a rotational band built on the ground state (g.s.). For the energy ratio $R_{10/2}$, Eq. (2) yields a linear plot of $R_{10/2}$ versus $R_{4/2}$ as shown in Fig. 3. The ratio $R_{10/2}$ varies from a value of 5.0 for a spherical vibrator to 18.33 for a deformed rotor. The deviations of the experimental data for the Nd isotopes from the linearity relation (2) for the energy ratio $R_{10/2}$ are exhibited here.

The soft rotor formula (SRF) (3) [18] expresses the variation in level energies in terms of the varying moment of inertia $\theta_I = \theta_0(1 + \sigma I)$,

$$E(I) = \hbar I(I+1)/2\theta_0(1+\sigma I), \tag{3}$$

which yields

$$R_{10/2} = (110/6)[3R_{4/2}/(40 - 9R_{4/2})]. \tag{4}$$

It is represented by the concave-shaped curve (dashed line) labeled SRF (Fig. 3). A third curve based on the power index formula [19],

$$E(I) = aI^b \tag{5}$$

is also drawn. Equation (5) yields the relation,

$$R_{10/2} = 5^b, \tag{6}$$

where the index $b = \log_{10} R_{4/2}/\log_{10} 2$.

In Fig. 3, I exhibit the data for Ba-Dy ($N > 82$). It is apparent that all data span the whole linearity curve and lie close on the lower side of it (see Ref. [20]).

Among the four data points at $R_{4/2} = 3.0$ [besides the $N = 92$ Ba (×), Sm, Gd (∇, ◯) lie highest, Dy, Nd (□, Δ) lie lower. The Ce, Ba (+, ×) ($N = 90$) lie lowest. These are the X(5) nuclei. On the other hand, at $N = 88$, Ba, Ce, and Nd lie higher than the other two isotones. See the cross (×) and plus (+) symbols for Ba and Ce and the Δ for Nd (at $R_{4/2} = 2.55$–2.7), respectively (labeled $N = 88$ in the central part). The $R_{10/2}$ data of Sm (∇), Gd (◯), and Dy (□) lie progressively much lower (labeled $N = 88$) in the lower part. The $N = 86$, Ba (×), Nd (Δ), and Sm,Gd data lie the lowest. The decrease in the ratio $R_{4/2}$ with increasing Z is usually explained on the basis of the $Z = 64$ subshell closure [4]. A microscopic view of this feature is given in Ref. [1].

B. The nonyrast levels

The spectral features of the nonyrast states present a picture vastly different from the features discussed above for the ground-state band (Fig. 4). At $N = 84$, the 2_2^+ state at 1560.9 keV is above the 4^+ ground state, but the 0_2^+ state lies too high at 2084.7 keV, that is at nearly $3 \times E(2_1^+)$ energy. The third 2^+ state lies below it. With $R_{4/2}$ less than 2.0, it is not a good collective vibration like pattern. A detailed analysis of the spectrum of ^{144}Nd *vis-à-vis* the microscopic theory of the pairing plus quadrupole model was given in Ref. [14].

At $N = 86$, the 0_2^+ state (at 1602.6 keV) descends below the 2_3^+ state, but the energy of the 2_2^+ state varies slowly with increasing N. Also its nature is that of the $K = 2$ quasi-γ band. The ground-state band energies vary sharply with N, and the 4_1^+ state is far below the higher excited states. The (4_1^+, 2_2^+, and 0_2^+) states do form a two-phonon triplet, but the higher states lie closely packed to form the three-phonon anharmonic multiplet. The state 4_2^+ lies below the 3_1^+ state (Table I). The collective structure of ^{146}Nd (along with other $N = 86$ isotones of Ce, Sm, and Gd) has been briefly analyzed in Ref. [16]. In this paper the special complex structures of the $N = 86$ isotones have been illustrated in the DPPQ model.

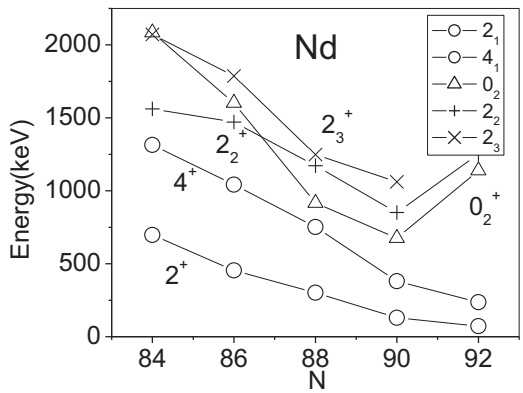

FIG. 4. The partial energy-level spectrum of $^{144-152}$Nd. At $N = 84$, 86 the 2_2^+ state is $K = 2$, 2_γ, but for $N = 88$–92 it is the $K = 0_2^+$ state.

TABLE I. The energy spectrum (upper rows) (in keV) [2] of $^{144-152}$Nd. The values from the DPPQ model (lower rows) are included.

State	$A = 144$	146	148	150	152
2^+	696.6	453.8	301.7	130.2	72.4
2^+ DPPQ	785	485[a]	307	129	86
4^+	1314.7	1042.2	752.3	381.1	236.6
4^+ DPPQ	1492	965	669	356.5	273
6^+	1791.5	1780.0	1279.8	720.2	484.0
6^+ DPPQ	2129	1493	1119	661.4	545
0_2^+	2084.7	1602.6	916.9	675.8	1139
0_2^+ DPPQ	1615	1061	947	941	1107
2_2^+	1560.9	1470.6	1171.0	850.8	1251.0
2_2^+ DPPQ	1843	1387	1333	1210	1227
2_3^+	2072.9	1787.3	1248.9	1062.1	
2_3^+ DPPQ	2525	1852	1624	1427	1497
3^+	2179.0	1777.2	1511.6	1200.6	1827[b]
3^+ DPPQ	2666	2050	1912	1575	1597
4_2^+	2109.8	1745.0	1604.1[c]	1137.8	1474.6
4_2^+ DPPQ	2440	1972	1787	1453	1422
4_3^+	2295.4	1918.5	1683.4	1352.5	1898[b]
4_3^+ DPPQ	3276	2505	2162	1743	1740
2_4^+		1905.3[d]	1659.9		
2_4^+ DPPQ		3069	2504		

[a]The slight increase in X_Q to 73.0 for ^{146}Nd yields $E(2_1^+) = 453$ keV, but higher spin energies are lowered.
[b]The 1827- and 1898-keV levels in ^{152}Nd are assigned $I^\pi = 3^+$ and 4^+ in Ref. [2].
[c]A 1604.1-keV state is assigned $I^\pi = 4^+$ in ^{148}Nd, but no I_γ intensities are listed [2].
[d]Two close-lying 2^+ states are at 1905.3 and 1978 keV in ^{146}Nd.

At $N = 86$–88, for the ground-state band, a mild shape phase transition is noted in Fig. 2, but the nonyrast states exhibit a very sharp change in the structure. The 0_2^+ state descends to the low value of ∼917 keV, and the character of the 2_2^+ state changes from the $K = 2$ to the $K = 0\beta$-vibrational state (Figs. 4 and 5). Now the 2_γ state lies above the 2_β state.

It is instructive to see the spectral changes with proton number Z at $N = 88$ (see Fig. 5). Although the ground-state band energies are rising with Z, the 0_2^+ state (and other higher ones) are descending with increasing Z. The increase in g.s. band energies with increasing Z is usually explained in terms of the $Z = 64$ subshell closure effects (leading to effective decreasing valence pair numbers or proton bosons). The descending 0_2^+ state provides a challenge to the application of IBM-1 or IBM-2. In terms of the Bohr-Mottelson geometrical framework, one can say that, although the nucleus is getting spherical, at the same time it is getting soft to axially symmetric β and γ vibrations.

III. THEORY

The phenomenological $L = 0, 2$ sd-IBM provides a useful guide to the variation in the collective nuclear structure of the

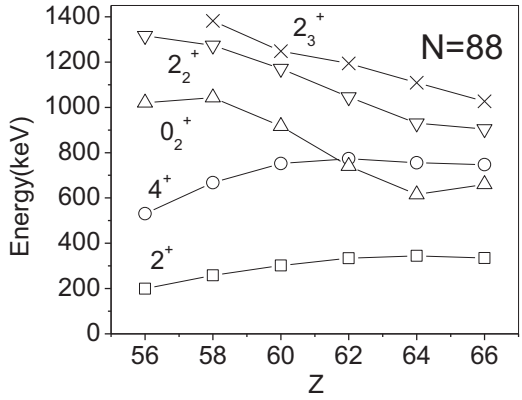

FIG. 5. $N = 88$ energy levels. The $2_2 = 2_\beta$ are correlated with 0_2^+, forming the $K^\pi = 0_2^+$ bands. The $2_3 = 2_\gamma$ states lie higher.

excited rotational vibrational bands. The four-term multipole expansion form $H_{\rm IBM}$ given by

$$H_{\rm IBM} = \varepsilon n_d + kQQ + k'LL + k''PP \qquad (7)$$

is adequate for the study of relative level energies and $B(E2)$ values. The quadrupole operator $Q^{(2)}$ is given by [3]

$$Q^{(2)} = (s^+d + d^+s) + \chi(d^+d)^{(2)}. \qquad (8)$$

The parameters of the IBM Hamiltonian require a fitting to the known energy-level data [including the specific $B(E2)$ values]. The computer program PHINT [21] is used for the calculation of the Hamiltonian in Eq. (7).

The microscopic dynamic pairing plus quadrupole model of Kumar-Baranger [13] is based on the basic concept of the Bohr-Mottelson geometrical model [22],

$$H_{\rm coll} = V(\beta,\gamma) + T_{\rm vib}(\beta,\gamma) + T_{\rm rot}(\beta,\gamma). \qquad (9)$$

The parameters of the collective Hamiltonian are derived microscopically from the $H_{\rm PPQ}$. It employs the basic quadrupole interaction between the particles-holes causing the deformation and the particle-particle pairing forces leading to the opposing spherifying effects. The PPQ Hamiltonian is given by Eq. (10),

$$H_{\rm PPQ} = H_{\rm sph} + H_Q + H_P. \qquad (10)$$

Starting from the spherical isotropic harmonic-oscillator energies and wave functions, one adds the quadrupole interaction to get the deformed single-particle energies and wave functions. Then the pairing interaction is added on equal footing in the HFB procedure to get the deformed quasiparticle energies and wave functions. From these, the parameters of the collective Hamiltonian are derived. The model is microscopic in the sense that no input energy-level data are required to set up the Hamiltonian $H_{\rm coll}$.

Only brief references to the previous study for ^{144}Nd in Ref. [14] and of ^{146}Nd in Ref. [16] are included here to provide a comprehensive view of the Nd isotopes. Also the relevant results of the IBM-1, for $^{144-150}$Nd of (1995) in Ref. [15] are included. The updated data over the past 20 years are included for the present IBM analysis.

IV. NUCLEAR STRUCTURE OF $^{144-152}$Nd IN THE IBM AND THE DPPQM

A. Energy levels and $B(E2)$ values

In my earlier study of Nd isotopes in the interacting boson model-1, the difficulty of (least-squares) fitting the ground-state band levels and the excited bands simultaneously was pointed out [15]. In fact, three different parameter sets of $H_{\rm IBM-1}$ were cited for ^{148}Nd. It was observed that the inclusion of the different numbers of the levels in the ground band along with the higher states gave different quality of fittings of the higher levels. At that time, the cause of this was not apparent. In the present paper, this problem is made more transparent (see the next paragraph). In several other empirical studies of the $N = 88$ (Nd,Sm,Gd) isotones the number of bosons were varied to take into account the $Z = 64$ subshell effects [23]. However, the disappearance of the $Z = 64$ subshell effects for the $N > 88$ isotopes indicates that the $Z = 64$ subshell is not due to a larger energy gap in the single-particle Nilsson orbitals of $\pi d_{5/2}$ (which completes the $Z = 64$ subshell at $\beta = 0$) and the $\pi h_{11/2}$ shell. In Ref. [1] I have presented a detailed explanation of the $Z = 64$ subshell effects and of its disappearance for $N > 88$.

Here, it is apparent that the $Z = 64$ subshell affects the static shape of the ^{148}Nd nucleus and its quasirotational ground-state band ($R_{4/2} = 2.50$), but its role in the vibrational states is more complex since the K-band formation into the β- and γ-vibrational bands is already exhibited here (see Figs. 4 and 5). So that just reducing the proton boson numbers N_p may not provide a full solution of the anomalous structure since the vibrational spectrum does not correspond to an anharmonic vibrator. The difficulty of a good fit simultaneously of the quasirotational band and the vibrational states is a real one in the phenomenological IBM. Even for the $N = 90$ ^{150}Nd nucleus such an anomaly is noted in Ref. [24] in reproducing the yrast levels and the $B(E2)$ simultaneously.

In Table I, the energy spectrum data [2] for $^{144-152}$Nd are given along with the DPPQM values. Although the ground-band level energies show a regular decrease with neutron number N, the $E(0_2^+)$ is minimum at ^{148,150}Nd. In general, in DPPQM, the ground band is slightly compressed (except in ^{144}Nd), and the vibrational bands lie higher. However, the basic pattern of ground band and excited

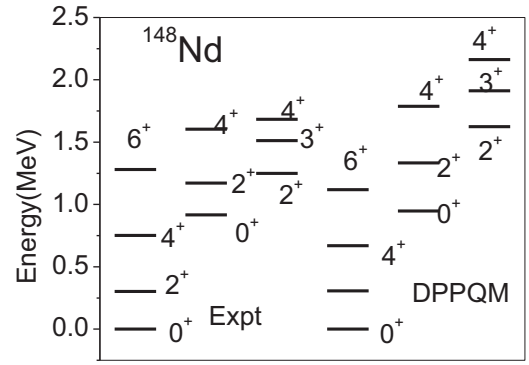

FIG. 6. Partial energy spectra of ^{148}Nd along with the DPPQ model predictions.

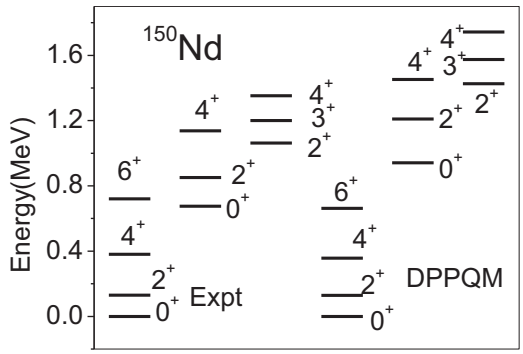

FIG. 7. Partial energy spectra of ^{150}Nd along with the DPPQ model predictions.

nonyrast bands is well reproduced (see Figs. 6 and 7 for ^{148,150}Nd). The minima of vibrational bands at $N = 88$–90 are predicted.

In Table II the variable parameters of the DPPQM and the calculated K-band structures of $I^\pi = 2^+$ states are given. The change in the nature of 2_2^+ and 2_3^+ states at $N = 88$ is reflected in their K-component structure. At $N = 88$ the second 2^+ state attains a predominant $K^\pi = 0^+$ character, and the 2_3^+ state attains the $K^\pi = 2^+$ character, although the K mixing is still large. Only in ^{150,152}Nd (at $N = 90, 92$) are almost pure K bands of β and γ bands formed. The DPPQ model parameter X_0 is the quadrupole strength factor in H_Q [Eq. (10)], which is varied by a few percent with N. The parameter F_B is the inertial core renormalization factor of the moments of inertia in $T_{\rm rot}$ and of the mass parameters of the vibration term $T_{\rm vib}$ of $H_{\rm coll}$ [Eq. (9)]. The same factor is used for both terms and varied within a factor of 2. The almost spherical nuclei ^{144,146}Nd require relatively larger X_0 and F_B parameters.

B. The potential-energy surface, static moments, and absolute $B(E2)$ values

In the DPPQ model [13], the potential-energy function of the nucleus is given by

$$V(\beta,\gamma) = \Sigma_i v_i^2 \eta_i - \Sigma_\tau g_\tau^{-1} \Delta_\tau^2 + (1/2)\chi^{-1}\beta^2.$$

Here i represents all the deformed quasiparticle (dqp) states of the two oscillator shells, v_i^2 are the occupation probability of a dqp state, η_i is the dqp energy, g_τ is the pairing strength ($\tau = n, p$), and Δ_τ is the calculated pairing gap. In the last term, the coefficient $\chi = X_0 \times A^{-1.4}$ MeV is the quadrupole force strength.

The calculated potential-energy curves $V(\beta, \gamma = 0^\circ)$ for $^{146-152}$Nd are illustrated in Fig. 8. For ^{146}Nd (also for ^{144}Nd), the PEC corresponds to a spherical vibrator (Fig. 8, upper left). For ^{148}Nd, the PEC has a minimum for $\beta > 0$ and lies on the

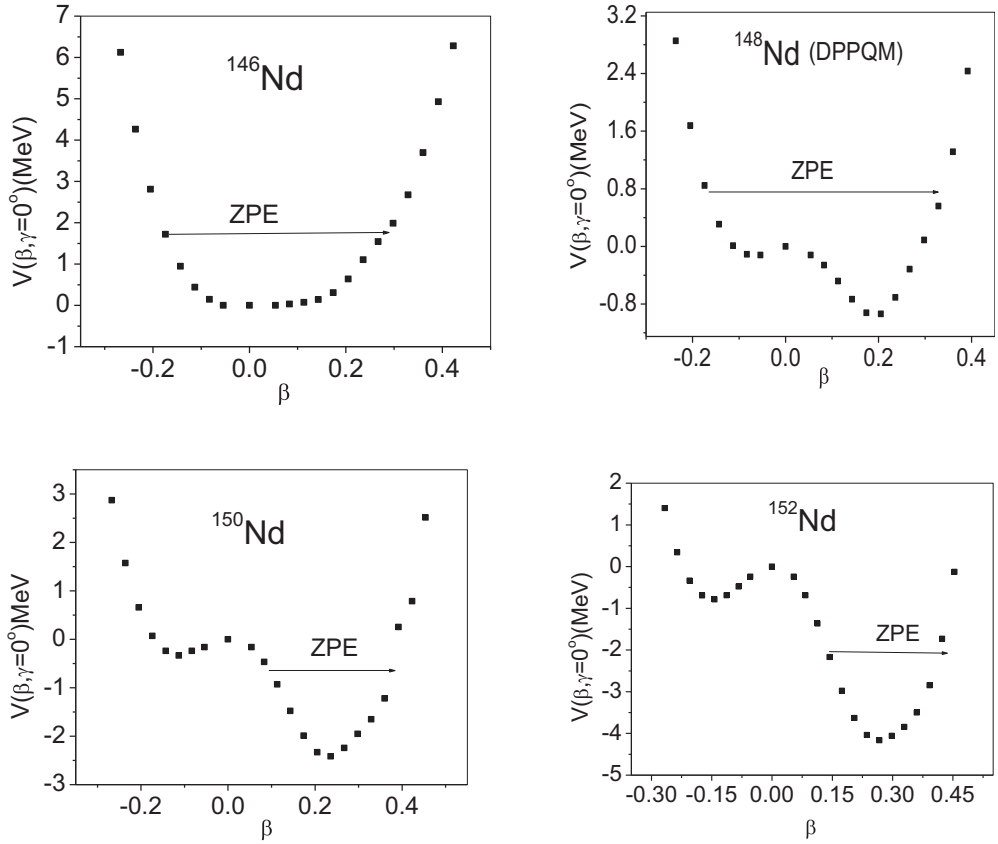

FIG. 8. The potential-energy curve $V(\beta, \gamma = 0^\circ)$ for $^{146-152}$Nd from the DPPQ model. The horizontal line labeled "ZPE" denotes the zero-point energy.

TABLE II. Parameters of the DPPQ model for Nd isotopes and the $K = 0$ components in percentages for $I^\pi = 2^+$ states. The proton charge parameter e_p is kept constant.

Parameter	144	146	148	150	152
$X_0(\text{MeV}^{-1})$	75.5	72.5	70.5	69.5	69.0
F_B	4.0	3.0	2.45	2.7	2.4
e_p	1.7	1.7	1.7	1.7	1.7
2_1^+	87	96.4	95.9	99.9	99.95
2_2^+	59[a]	43.7[a]	64	94.1	99.03
2_3^+	52[a]	57.4[a]	38	6.3	1.06

[a]In ^{144,146}Nd, no proper excited K bands are formed.

TABLE III. Some static moments in Nd isotopes. V_{def} and V_{PO} are in MeV.

$A =$	144	146	148	150	152
$R_{4/2}$	1.887	2.30	2.498	2.927	3.263
β_{min} DPPQM	0	0	0.205	0.236	0.267
β_{rms} (g.s.)	0.134	0.156	0.194	0.240	0.275
β_2 [26]	0.1241	0.1522	0.2014	0.285 21	0.349 12
γ_{rms} (g.s.)	28°	25°	0.20°	15°	13°
V_{def}	0.0	0.0	0.936	2.414	4.16
V_{PO}	0.0	0.0	0.817	2.18	3.375

prolate side at $\beta = 0.2$ with a depth V_{def} below the spherical barrier of 0.94 MeV and a shallow oblate minimum at $\beta = 0.1$ (Fig. 8, upper right). The ZPE, indicated by the horizontal line, is 0.79 MeV above the spherical barrier and extends from $\beta = -0.17$ to $+0.33$. This explains its anharmonic vibrator structure and the larger K admixture in the higher $I^\pi = 2^+$ states.

For ^{150}Nd, the PEC (Fig. 8, lower left) lies at $\beta = 0.236$, with a depth V_{def} of 2.4 MeV and oblate minimum at $\beta = 0.11$ and depth of 0.24 MeV. The zero-point energy level is 0.63 MeV below the spherical barrier and extends from $\beta = 0.11$ to 0.36 in the prolate minimum. The β_{rms} is 0.24, and $\gamma_{\text{rms}} = 15°$. Thus the nucleus is quite soft to fluctuations in the β variable. This is in consonance with the low-lying 0_2^+ state along with the 2_2^+ state in ^{148,150}Nd. For ^{152}Nd, V_{def} is still larger (Fig. 8, lower right). These different PECs for the $N = 86 - 92$ isotopes provide an insight of the difference in their structures. The main characteristics of these potential-energy surface (PES) plots including V_{def}, V_{PO} (the difference between the prolate and the oblate minima), and deformation β_{min}, β_{rms} are listed in Table III.

The quadrupole deformation parameter β_2 increases with N. The β_{min} of the PEC is zero for ^{144,146}Nd, but the β_{rms} is greater than zero. The γ_{rms} is close to 30°. For ^{148}Nd the β_{min} is 0.205, and for ^{152}Nd, β_{min} shifts to 0.267. The β_{rms}'s are larger. The latter are closer to β_2 [derived from, $B(E2), 2_1^+ - 0_1^+$)] from experiment. Calculated V_{def} and V_{PO} affect the $E(2_\gamma)$–$E(4_1^+)$ energy gap of the spectra [25].

In Table IV, some $E2$, $M1$, and $E0$ moments predicted in the DDPQ model are also given. The quadrupole moment $Q(2_1^+)$ is a good measure of the structural changes with N. In the DPPQ model, these variations are well reproduced Magnetic moments $\mu(2_1^+)(nm)$ from the DPPQ model are compared with data [2]. The magnetic moments exhibit slow variation with A (except for ^{144}Nd) corresponding to $g(2_1) = Z/A$ values. The DPPQM also gives the slow variation with A. The electric monopole moments for the $2_2^+ - 2_1^+$ transition are increasing with increasing N. The value is negative for the anharmonic vibrator nucleus ^{146}Nd. The same is true for the $E0$ amplitude for the $2_3^+ - 2_2^+$ transition, indicating a phase difference in their wave functions.

The larger values of $\rho(E0)$ at $N = 90, 92$ reflects the β-vibrational nature of the 2_2^+ state. For the $2_3^+ - 2_1^+$ transitions, it is decreasing, which is an indication of the lesser β-γ band

TABLE IV. Quadrupole moments (eb), magnetic moments, electric monopole transition matrix elements, and $B(E2)$'s in e^2b^2 for $^{146-152}$Nd.

A	144	146	148	150	152
$Q(2_1^+)$ expt.[a]	− 0.635 3	− 0.79 2	− 1.05 2	− 1.50 1	− 1.85 6
DPPQM	− 0.48	− 0.89	− 1.21	− 1.50	− 1.71
$\mu(2_1^+)(nm)$ expt[b]	0.30 2	0.58 2	0.64 8	0.64 2	
DPPQM	0.51	0.54	0.63	0.56	0.61
$\rho(E0)(2_2–2_1)$	0.23	− 0.34	0.55	0.73	0.80
$(\rho(E0)(2_3–2_1)$	0.10	0.32	0.40	0.17	0.06
$X(E0/E2E)0_2^+ - 2_1^+$	0.027	0.074	0.17	0.47	1.14
$B(E2,0_1^+ - 2_1^+)$[a]	0.491 5	0.760 23	1.37 2[b]	2.72 2[b]	4.20 28[c]
DPPQM	0.69	1.05	1.72	2.73	3.60
$B(E2,0_1^+ - 2_2^+)$	0.0030 4[d]	0.073 2[d]	0.020 2[b]	0.012 1[b]	
DPPQM	0.027	0.056	0.033	0.004	0.024
$B(E2,0_1^+ - 2_3^+)$			0.073 3[b]	0.072 3[b]	
DPPQM	8×10^{-5}	0.007	0.064	0.115	0.110

[a]Reference [26].
[b]Reference [2].
[c]Previous tabulation of Raman *et al.* At. Data and Nucl. Data Tables 36, 1 (1987) was of 2.6 (7).
[d]Deduced from Ref. [28].

TABLE V. The absolute $B(E2)$ values (in e^2b^2) in ^{148,150}Nd.

		^{148}Nd			^{150}Nd				
I_i	I_f	Expt [2].	IBM [15]	DPPQ	Expt [2].	Expt [6].	IBM [15]	DPPQ	X(5)[a]
0_1^+	2_1^+	1. 37 2	1.37	1.37	2.72 2	2.72	2.72	2.72	2.72
	2_2^+	0.020 3	0.002	0.026	0.012 1	0.0065	0.068	0.004	0.054
	2_3^+	0.073 3	0.039	0.051	0.072 3	0.080 20	0.084	0.115	0.079
0_2^+	2_1^+	0.013 5	0.013	0.31	0.21 1	0.21 1	0.13	0.21	0.34
2_2^+	2_1^+	0.085 5	0.0105	0.09	0.034 5	0.049 11	0.10	0.041	0.047
2_3^+	2_1^+	0.026 6	0.009	0.017	0.032 5	0.029 4	0.009	0.038	0.025
4_1^+	2_1^+	0.44 1	0.38	0.49	0.84 6	0.99 1	0.80	0.84	0.86
2_2^+	0_2^+		0.165	0.22	0.45 15	0.62 12	0.22	0.49	0.43
$E2SD$			0.12				0.16		
$E2DD$			− 0.20				−0.20		

[a]X(5) symmetry values normalized to $B(E2, 0_1–2_1)$ from Refs. [6,29].

TABLE VI. Interband $B(E2)$ ratios in ^{144}Nd. The level energy and E_γ are in keV. $\varepsilon = 644.8$, $2k =$ variables QQ $= -8.4$, ELL $= 2k' = -30.6$, PAIR $= k''/2 = -33.2$ keV, $e_b = 0.16$, and $E2DD = -0.20$. In PHINT QQ $= 2k$, ELL $= 2k'$, PAIR $= k''/2$, and $E2DD = e_b\chi$.

E (keV)	I_i	$I_f/I_{f'}$	$E_{\gamma1}/E_{\gamma2}$	Expt. [2]	IBM-1	DPPQ
1560.9	2_2^+	0/2	1561/864	0.050 (2)	0.003	0.035
2072.9	2_3^+	0/2	2073/1376	0.055 2	<0.07	0.00004
2179.0	3_1^+	2/4	1482/864	0.038 3	0.017	0.082
2109.8	4_2^+	2/4	1413/795	0.82 6[a]	0.007	0.12
2295.4	4_3^+	2/4	1599/981	0.014 2	<0.04	0.0004
		2_2/4	735/981	0.31 8	0.002	0.03

[a]Using the relative I_γ from Ref. [30].

TABLE VII. $B(E2)$ ratios in β-g,γ-g transitions in ^{146}Nd. The level energy and E_γ are in keV. $\varepsilon = 836.7$, $2k =$ QQ $= -28.0$, ELL $= 2k' = 26.1$, PAIR $= k''/2 = 22.3$ keV, $e_b = 0.13$, and $E2DD = -0.25$.

E (keV)	I_i	$I_f/I_{f'}$	$E_{\gamma1}/E_{\gamma2}$	Expt. [15]	Expt. [2]	IBM [15]	DPPQ
1470.6	2_2^+	0/2	1471/1017	0.15 2	0.15 1	0.011	0.074
1745.0	4_2^+	4/2	702/1292	53.6 60	54 8	104	18
1777.2	3_1^+	4/2	736/1323	10 1	0.70 7[a]	17	2.5
1787.3	2_3^+	0/2	1787/1333	0.029 5	0.029 3	>1	0.12
1905.3	2_4^+	0/2	1905/1651	0.005 1	0.005 1	>0.5	0.012
1918.5	4_3^+	4/2	876/1465	12.4 14	13 1	8	28.6
		$2_2/2_1$	448/1465	228 24	236 60	25	0.7

[a]The previous value of 10 (1) is from Ref. [31]. There is an uncertainty in the $B(E2)$ ratio due to the $M1$ component.

TABLE VIII. $B(E2)$ ratios in β-g,γ-g transitions in ^{148}Nd. The level energy and E_γ are in keV. $\varepsilon = 356.3$, $2k = \text{QQ} = -45.4$, $2k' = \text{ELL} = 36.6$, and $k''/2 = \text{PAIR} = 7.0$ keV, $e_b = 0.12$, and E2DD $= -0.20$.

E (keV)	I_i	$I_f/I_{f'}$	$E_{\gamma1}/E_{\gamma2}$	Expt. [15]	Expt. [2]	IBM [15]	DPPQ
1171.0	2_2^+	0/2	1171/869	0.034 8	0.037 6	0.04	0.068
		2/4	869/418		0.92 46	2.65	1.12
1248.9	2_3^+	0/2	1249/947	0.60 12	0.57 6	0.90	0.61
		2/4	847/497		0.35 25	1.93	0.41
1511.6	3_1^+	4/2	759/1210	2.31 46	2.32 40	1.09	1.22
1604.1	4_2^+	2/4	1302/852			0.028	0.004
		2_2/4				17.4	8.7
1683.4[a]	4_3^+	2/4	1381/933		1.57 68	0.39	2.95
		2_2/4	512/933		34 30	2.07	0.006
		2_3/4				20.5	12.4

[a]A 1604.1-keV $I = 4$ level is listed without I_γ values for the $E2$ transitions.

mixing [27] in ^{150,152}Nd. The $X(E0/E2)(0_2^+ - 2_1^+)$ factor varies with N with a maximum in ^{150,152}Nd, indicating a purer β band. All the parameters of the DPPQ model calculation are kept constant, except the ones listed in Table II.

The increase in the absolute $B(E2,0_1^+ \to 2_1^+)$ with neutron number N is well given in the DPPQ model with constant charge parameter ($e_n = 0.7$) ($e_p = 1 + e_n$). In contrast, in IBM-1 the boson charge e_b of the $E2$ transition operator $T(E2) = e_b \times Q^{(2)}$ has to be varied with N [15] as listed in the tables below. The larger $B(E2,0_1^+ - 2_2^+)$ at $N = 86$ than for heavier isotopes supports the change in the character of the 2_2^+ state from $K = 2$ at $N = 86$ to $K = 0$ at $N = 88$–90. A complementary change takes place for the 2_3^+ state.

C. Absolute $B(E2)$ values in ^{148,150}Nd

The predictions of the absolute $B(E2)$ values from the model (Table V) provide useful tests of the applicability of the model to the nucleus. In ^{148}Nd, the absolute $B(E2,0_1^+ \to 2_2^+)$ is smaller than $B(E2,0_1^+ \to 2_3^+)$ indicating $2_2^+ = 2_\beta$ and $2_3^+ = 2_\gamma$, as also given in IBM-1 and the DPPQ model. In all cases, the $B(E2)$ values from the DPPQ model are closer to experiment than in IBM-1. The values are normalized to $B(E2,0_1^+ \to 2_1^+)$ for a better comparison.

In ^{150}Nd also, the absolute $B(E2,0_1^+ - 2_2^+)$ is smaller than $B(E2,0_1^+ - 2_3^+)$, indicating $2_2^+ = 2_\beta$ and $2_3^+ = 2_\gamma$, as also given in IBM-1 and the DPPQ model. Again the DPPQ model values are in better agreement with experiment than IBM-1 values in most cases. The ratio $B(E2,4-2)/B(E2,2-0)$ is 1.5 in ^{148}Nd and 1.6 in ^{150}Nd. The other $B(E2)$ ratios are well given The X(5) symmetry values [6] are in fair agreement with experiment. Values for the 2_3^+ states are from Ref. [29].

D. The interband $B(E2)$ ratios

The calculated interband $B(E2)$ ratios for $^{144-152}$Nd are listed in Tables VI–X. The data as available in 1995 for Ref. [15] and the updated present data are listed. Also the IBM-1 values of Ref. [15] are included for comparison with the DPPQ model results.

In ^{144}Nd (Table VI), the $B(E2)$ ratios for $E2$ transitions to the ground band are listed. There are differences in the IBM-1 and DPPQ model values, but on the average the DPPQM values are better.

In ^{146}Nd (Table VII), the calculated $B(E2, 2_2\text{–}0/2)$ and $B(E2, 2_3\text{–}0/2)$ ratios from the DPPQ model agree with data within a factor of 2, much improved in comparison with the

TABLE IX. $B(E2)$ ratios in β-g,γ-g transitions in ^{150}Nd. The level energy and E_γ are in keV. $\varepsilon = 464.3$, $\text{QQ} = -31.4$, $\text{ELL} = 1.4$, $\text{PAIR} = 10.0$ keV, $e_b = 0.16$, and E2DD $= -0.20$.

E (keV)	I_i	$I_f/I_{f'}$	$E_{\gamma1}/E_{\gamma2}$	Expt [2].	Expt [6].[a]	IBM [15]	DPPQ	X(5)[b]
850.5	2_2^+	0/2	850/720	0.070 30	0.13 5	0.14	0.018	0.22
		4/2	470/720	1.96 20	1.89 76	0.10	1.99	4.1
		0_2/4	174/470	8.6 60	6.7 27	23.6	6.0	9.1
1061.4	2_3^+	0/2	1061/932	0.55 14	0.56 30	1.96	0.60	0.66
		4/2	680/932	0.31 24	0.48 40	5.5	0.35	0.05
1200.6	3_1^+	4/2	819/1070	0.80 28		1.09	0.82	0.42
1137.8	4_2^+	4/2	756/1007	910 270	58 18	26.5	24	5.7
		2/4	1007/756	0.0011 4	0.017 7	0.038	0.043	0.17
		2_2/4	287/756	1.6 7	24 11	5.5	22	20
1352.5	4_3^+	4/2	972/1223	8.1 20	4.3 24	2.0	3.4	3.2
		2_3/4	290/972	27 7		27	105	

[a]Values from Ref. [6] are from the lifetime measurements.
[b]β-g values are from Ref. [6], and γ-g values are from Ref. [29].

TABLE X. $B(E2)$ ratios in β-g,γ-g transitions in ^{152}Nd. The level energy and E_γ are in keV. $\varepsilon = 472.0$, QQ $= -58.4$, ELL $= -10.6$, PAIR $= -14.0$ keV, $e_b = 0.145$, and $E2DD = -0.20$.

E (keV)	I_i	$I_f/I_{f'}$	$E_{\gamma1}/E_{\gamma2}$	Expt.	IBM	DPPQM
1251.0	2_2^+	0/2	1251/1178	0.21 4	0.167	0.215
		4/2	1014/1178	2.83 28	2.70	2.85
1474.6	4_2^+	4/6	1238/990	0.37 10	0.78	0.37
1827.1	3^+	2/4	1754/1591	1.96 50	1.56	1.40
1898.0	4_3^+	2/4			0.21	0.23
	2_3^+	0/2			0.57	0.58
		2/4			13	7.9
1893.9	$3, 4^+$	2/4	1821/1658	5.2 13		

IBM values [14]. The weak $B(E2, 2_4\text{–}0/2)$ ratio is also well given in the DPPQM. The $B(E2)$ ratio for 1777-keV 3^+ in the DPPQM differs by a factor of 3 from the revised value [2] (see footnote in Table VII). The DPPQ model values are closer to the data than the IBM-1 values, including the $B(E2)$ ratio for the 4_2^+ state. But the $B(E2, 4_3^+\text{–}2_2/2_1)$ ratio is not reproduced in the DPPQM.

In ^{148}Nd (Table VIII), the calculated $B(E2, 2_2\text{–}0/2)$ and $B(E2, 2_3\text{–}0/2)$ ratios from the DPPQ model and IBM-1 agree with data and support the 1171-keV $2_2 = 2_\beta$ and 1249-keV $2_3 = 2_\gamma$ assignments. The IBM-1 values for the other $B(E2)$ ratios from the $I = 2$ states and 3_1^+ are in better agreement with the data than that obtained in the lighter isotope. The 1604-keV level is assigned to $I^\pi = 4^+$ in Ref. [2], but no I_γ values for $E2$ transitions to 2_1^+ and 4_1^+ are listed. Ibbotson *et al.* [32] in their Coulomb excitation work listed an $E3$ transition from 1604 to 1023 keV. Also a 2149-keV 6_β level is listed in Refs. [2,32], again without I_γ values. The 1683-keV 4^+ decays to 2_g and 4_g yielding $B(E2, 4\text{–}2/4) = 1.57$ (68) and to the 1171-keV 2_β state. But the error margin in the $B(E2)$ ratio is large.

For ^{148}Nd, the $B(E2, 4_2\text{–}2/4)$ in the DPPQM and IBM-1 is small, and $B(E2, 4_3\text{–}2/4)$ is 0.4 and 3.0, respectively. The $B(E2, 4_2\text{–}2_2/4_1)$ is large in theory. But for $B(E2, 4_3\text{–}2_2/4_1)$ IBM and the DPPQM results differ. Thus from the available data on the $I^\pi = 4^+$ states, the association of 1604- and 1683-keV states with model 4^+ states remains ambiguous.

In ^{150}Nd (Table IX), the weak $B(E2, 2_2^+\text{–}0/2)$ and the much larger $B(E2, 2_3^+\text{–}0/2)$ support their $K = 0_2$ and $K = 2$ characters as also indicated in the IBM and DPPQM. The X(5) value for the $B(E2, 2_2\text{–}0/2)$ of 0.22 is larger than experiment by a factor of 2. For other $B(E2)$ ratios from these states, the DPPQ model values are in better agreement with the data. The revised $B(E2, 3^+\text{–}4/2)$ value is given better in the DPPQM. Similar fair agreement is obtained for the transitions from the $I^\pi = 4^+$ states. $B(E2, 4_2\text{–}2/4)$ is 0.17 in X(5) symmetry and is again larger than the DPPQM and IBM-1 values [24]. It is worth noting that the relative strength of the $E2$ transitions from the 4_2^+ to the 2_1^+ and 4_1^+ changes drastically for ^{148}Nd to ^{150}Nd in experiment, which is not reproduced in theory. There is also the problem of the identification of the 1604.1-keV $I = 4^+$ state in ^{148}Nd.

In ^{152}Nd (Table X), the weak $B(E2, 2_2\text{–}0/2)$ supports its $K = 0_2$ character of the second $I^\pi = 2^+$ state. Both $B(E2)$ ratios from the 2_2^+ state are well given in the DPPQM and IBM. The same is well obtained for the second $I^\pi = 4^+$ state. The $2_3 = 2_\gamma$ is not yet assigned from experiment. From the DPPQ model I get the larger $B(E2, 2_3\text{–}0/2)$ value of 0.58, closer to the Alaga value of 0.70, as expected for a $K = 2$ state, *vis-à-vis* the $B(E2, 2_2\text{–}0/2)$ value of $= 0.215$ which is farther from the Alaga value of 0.70. Similar values are obtained in IBM-1. In the National Nuclear Data Center [2], a 1827-keV $I^\pi = 3^+$ state is listed which decays to 2_g and 4_g states. The calculated $B(E2)$ ratio agrees with the DPPQ model and IBM-1 values. No $I^\pi = 2^+$ state of this band is listed in Ref. [2]. The listed 4^+ at 1898.0 keV decays to 4_g only in the ground band. So no $B(E2)$ ratios from experiment are listed. Also a level at 1893.9 keV is assigned the ambiguous spins of 3^+ or 4^+. So we cannot assign any spin to it from theory.

E. Role of protons and neutrons for shape phase transition

As explained in Sec. III A, from the solution of the PPQ Hamiltonian, I get the quasiparticle energies and wave functions. Therein I also calculate the occupation probabilities of neutrons and protons in the deformed Nilsson orbits. In Table XI, I list the occupation numbers of the $\nu f_{7/2}$, $\nu h_{9/2}$, and $\nu i_{13/2}$, which lie lowest for neutrons, and $\pi g_{7/2}$, $\pi d_{95/2}$, and $\pi h_{11/2}$ for protons. The other orbits contribute only small amounts. The occupation of ten protons of Nd above the $Z = 50$ shell varies slightly with N. A slight shift from the lower orbits to $h_{11/2}$ occurs at $N = 86$–90. The increasing filling of neutrons in the down-sloping neutron orbits cooperating with protons produces the deformation. From the table it appears that the increased filling of the $\nu h_{9/2}$ orbit at $N = 86$–88 provides the small deformation at $N = 88$, and the additional filling of the $\nu i_{13/2}$ orbits triggers the shape transition at $N = 88$–90 (mild relative to Sm,Gd, as illustrated in Fig. 1). The effect of the n-p interaction of the $\pi h_{11/2}$ and

TABLE XI. The occupation numbers of protons and neutrons in Nilsson orbits at $\beta = 0$ for ^{146}Nd, $\beta = 0.205$ for ^{148}Nd, and $\beta = 0.236$ for ^{150}Nd calculated in the DPPQ model.

Orbit	$A = 146$	148	150	Orbit	$A = 146$	148	150
$\nu f_{7/2}$	1.684	2.018	2.286	$\pi g_{7/2}$	4.038	3.648	3.542
$\nu h_{9/2}$	1.399	2.180	2.684	$\pi d_{5/2}$	2.559	2.273	2.182
$\nu i_{13/2}$	0.717	0.638	1.446	$\pi h_{11/2}$	2.657	2.947	3.069
Sum	3.800	4.836	6.416	Sum	9.254	8.868	8.793
$N = 82$	4	6	8	$Z = 50$	10	10	10

$\nu h_{9/2}$ orbitals, along with the contribution of the $\nu i_{13/2}$ orbital, leads to the sharp phase transition at $N = 88$–90 (see Ref. [1]).

V. DISCUSSION AND CONCLUSION

With increasing N, the collective K-band formation evolves in the Nd isotopes. With the help of the empirical data on the ground band, I have illustrated the special status of the Nd isotopes *vis-à-vis* the (Ba,Ce) and (Sm,Gd) isotones for $N = 86, 88$, and 90. Here the effect of the $Z = 64$ subshell is evident. This is in accord with the variation in the PESs illustrated by Li *et al.* [11]. The variation in the energy spectra with N is also well illustrated by Giannatiempo in Ref. [8].

In the present paper, I have illustrated the very interesting complex structure of the $N = 86, 88$ isotopes in the excited $K = 0_2^+$, $K = 2$ bands, which explains the difficulty in the simultaneous fitting of data for the ground and the excited bands as also experienced in the IBM-2 [8] and IBM-1 studies [24] of Nd isotopes. However, in the dynamic PPQ model where the intrinsic microscopic structure is involved, this difficulty is mitigated to some extent, and the model predicts the $B(E2)$ values and the interband $B(E2)$ ratios in ^{148,150}Nd in fair agreement with experimental data. The variation in the $B(E2)$ values is achieved here with constant charge parameter $e_n = 0.7$ ($e_p = 1 + e_n$) as distinguished from the variation in boson charge in the IBM-2 study of Ref. [8] and in my IBM-1 calculation. The shape changes at $N = 86$–88 and $N = 88$–90 are also illustrated through the PEC for the three isotopes. The variation in $E2$, $M1$, and $E0$ components with N are illustrated. I have also illustrated the role of neutron and proton filling in producing the shape transition. Besides the static shape of the nucleus affecting the ground band, the dynamics of the nuclear motion affecting the excited bands is illustrated.

ACKNOWLEDGMENTS

J.B.G. appreciates the postretirement association with Ramjas College.

[1] J. B. Gupta, Phys. Rev. C **87**, 064318 (2013).
[2] Brookhaven National Laboratory, Chart of nuclides of National Nuclear Data Center [http://www.nndc.bnl.gov/ENSDF].
[3] F. Iachello and A. Arima, *The Interacting Boson Model* (Cambridge University Press, Cambridge, UK, 1987).
[4] R. F. Casten, D. D. Warner, D. S. Brenner, and R. L. Gill, Phys. Rev. Lett. **47**, 1433 (1981).
[5] F. Iachello, Phys. Rev. Lett. **87**, 052502 (2001).
[6] R. Krucken *et al.*, Phys. Rev. Lett. **88**, 232501 (2002).
[7] R. M. Clark, M. Cromaz, M. A. Deleplanque, R. M. Diamond, P. Fallon, A. Görgen, I. Y. Lee, A. O. Macchiavelli, F. S. Stephens, and D. Ward. Phys. Rev. C **67**, 041302 (2003).
[8] A. Giannatiempo, Phys. Rev. C **84**, 024308 (2011).
[9] A. Giannatiempo, L. Fortunato, and A. Vitturi, Phys. Rev. C **86**, 034311 (2012).
[10] N. Turkan and I. Inci, Phys. Scr. **75**, 515 (2007).
[11] Z. P. Li, T. Nikšić, D. Vretenar, J. Meng, G. A. Lalazissis, and P. Ring, Phys. Rev. C **79**, 054301 (2009).
[12] L. M. Robledo, R. R. Rodríguez-Guzmán, and P. Sarriguren, Phys. Rev. C **78**, 034314 (2008).
[13] K. Kumar and M. Baranger, Nucl. Phys. A **110**, 529 (1968).
[14] J. B. Gupta, Nucl. Phys. **A484**, 189 (1988).
[15] J. B. Gupta, J. Phys. G: Nucl. Part. Phys. **21**, 565 (1995).
[16] J. B. Gupta, Eur. Phys. J. A **50**, 176 (2014).
[17] J. B. Gupta and M. Saxena, Phys. Rev. C **91**, 054312 (2015).
[18] P. von Brentano, N. V. Zamfir, R. F. Casten, W. G. Rellergert, and E A McCutchan, Phys. Rev. C **69**, 044314 (2004).
[19] J. B. Gupta, A. K. Kavathekar, and R. Sharma, Phys. Scr. **51**, 316 (1995).
[20] J. B. Gupta, Int. J. Mod. Phys. E **22**, 1350064 (2013).
[21] O. Scholten, Computer program package PHINT.
[22] A. Bohr and B. R. Mottelson, *Nuclear Structure* (Benjamin, New York, 1975), Vol. 2.
[23] R. L. Gill, R. F. Casten, D. D. Warner, D. S. Brenner, and W. B. Walters, Phys. Lett. **118**, 251 (1982).
[24] E. A. McCutchan, N. V. Zamfir, and R. F. Casten, Phys. Rev. C **71**, 034309 (2005).
[25] K. Kumar, Phys. Rev. C **1**, 369 (1970).
[26] S. Raman, C. W. Nestor, Jr. and P. Tikkanen, At. Data Nucl. Data Tables **78**, 1 (2001).
[27] E. A. McCutchan and R. F. Casten, Phys. Rev. C **77**, 054320 (2008).
[28] C. Fahalander, A. Backlin, L. Hasselgen, C. Pomar, G. Possnert, and J. E. Thun, Inst. Phys. Conf. Ser. **49**, 291 (1980); (private communication).
[29] R. Bijker, R. F. Casten, N .V. Zamfir, and E. A. McCutchan, Phys. Rev. C **68**, 064304 (2003).
[30] J. K. Tuli, Nuclear Data Sheets **56**, 607 (1989).
[31] D. M. Snelling and W. D. Hamilton, J. Phys. G: Nucl. Part. Phys. **9**, 111 (1983).
[32] R. Ibbotson *et al.*, Phys. Rev. Lett. **71**, 1990 (1993).